Journal of Materials Chemistry A

RSC Publishing

PAPER

Investigation of the anti-biofouling properties of graphene oxide aqueous solutions by electrowetting characterization†

Cite this: *J. Mater. Chem. A*, 2013, **1**, 12355

Guillaume Perry,‡[ab] Yannick Coffinier,[a] Rabah Boukherroub[a] and Vincent Thomy*[b]

Received 3rd July 2013
Accepted 14th August 2013

DOI: 10.1039/c3ta12576a

www.rsc.org/MaterialsA

In this study, we investigate the anti-biofouling properties of graphene oxide (GO) nanosheets with bovine serum albumin (BSA). These properties are characterized by contact angle hysteresis (CAH) measurements and contact angle (CA) modification under electrowetting (EW), in order to determine the surface modification due to BSA adsorption. The experiments show two different behaviors. The droplets containing only BSA or BSA with low GO concentration exhibit high CAH and irreversible CA modification under EW due BSA adsorption on the surface. However, in the presence of a high GO concentration, the CAH is largely lowered and CA modification under EW is reversible, suggesting preferential adsorption of BSA on GO nanosheets.

Introduction

The miniaturization of diagnostic systems, also known as lab-on-chip, has led to much more efficient, faster, and sensitive bio-detection or analysis. The advent of these systems has been widely reported since the 90s. However, there are still many barriers to their widespread deployment such as lack of standardized processes in technology. Despite the various proofs of concept already made for biological applications,[1–3] the major problem encountered is due to the increased surface to volume ratio.[4] At the microscopic scale, surface effects (capillarity, viscosity, *etc.*) are dominant over volume effects (gravity). When biological or biochemical interactions are considered, the surface effects become a big advantage because nanometer sized sensors present a huge surface of contact. However, they can also give rise to the enhancement of the interaction[5] between the fluid containing biomolecules and the surface, which could promote bio-pollution due to nonspecific adsorption of biomolecules. While this phenomenon appears also at the macroscopic scale, at this scale it has much more serious consequences: loss of biomolecules and thus a change of concentration, cross contamination, modification of surface properties and even obstruction of microfluidic channels.[6] It is, therefore, necessary to monitor the liquid–surface interaction to limit the uncontrolled adsorption of biomolecules on the surface. Looking at the microfluidic side, nonspecific adsorption is detrimental to the surfaces and should be avoided. As far as digital microfluidics is concerned, the surface property is crucial for the physical phenomenon of EWOD (electrowetting on dielectric), which is largely described in the literature for pure conductive liquids.[7] Briefly, the application of a voltage between a conductive droplet and an electrode, covered by an insulating hydrophobic layer, leads to the modification of the apparent contact angle of the droplet. The reversibility of this modification strongly depends on the surface properties at the triple contact line of the droplet.[8]

However, the fluids used for lab-on-chip applications are most of the time complex fluids containing ions and macromolecules (proteins). Displacing these liquids with EWOD in air often leads to the same behavior: non-specific adsorption of biomolecules, pinning of the triple line and non-reversibility of the contact angle modification by EWOD. While different strategies have been developed to balance this non-specific adsorption (modulation of the applied voltage,[8] use of surfactants as core–shell like,[9–11] oil as biphasic medium[12–14] or superhydrophobic surfaces[15,16]), these techniques cannot really preserve the intrinsic versatility of EWOD because all of them are focused on the droplet–surface interaction and not on the liquid itself, preventing or making difficult ligand–target interactions. In our previous paper,[17] we proposed to use graphene oxide (GO) nanosheets as nanocargoes for biomolecules due to their high binding strength with amino acids[18] and proteins,[19] which is already used for various applications.[20–22] Although for graphene–DNA interactions, π–π bonding plays a major role, H-bonding and electrostatic interactions are

[a]*Institut de Recherche Interdisciplinaire (IRI), USR CNRS 3078, Université Lille 1, Parc de la Haute Borne, 50 Avenue de Halley, BP 70478, 59658 Villeneuve d'Ascq, France*
[b]*Institut d'Electronique, de Microélectronique et de Nanotechnologie (IEMN), UMR CNRS 8520, Université Lille 1, Cité Scientifique, Avenue Poincaré, CS 60069, 59652 Villeneuve d'Ascq, France. E-mail: Vincent.thomy@iemn.univ-lille1.fr; Fax: +33 3 30 19 78 98; Tel: +33 3 20 19 79 51*

† Electronic supplementary information (ESI) available. See DOI: 10.1039/c3ta12576a

‡ Present address: LIMMS/CNRS-IIS, Institute of Industrial Science, University of Tokyo, 4-6-1 Komaba, Meguro-ku, Tokyo 153-8505, Japan.

believed to be the main bonds involved in protein–GO interactions. Thus, GO has higher binding affinity for proteins compared to graphene (or reduced graphene oxide), because of its high content of oxygen functional groups. We have characterized GO–BSA interactions in aqueous droplets through contact angle (CA) measurements under evaporation. For a [BSA]/[GO] ratio of about 0.7, BSA adsorbs preferentially on GO without any visible surface pollution (droplet triple line slips, stable CA). Under these conditions, it was possible to perform long-term displacement of droplets by EWOD.

The present paper is an extension of our previous work and is focused on the study of GO nanosheets to prevent biofouling in microfluidic systems. The GO nanosheets are mixed with BSA at different GO/BSA ratios; this protein is chosen as a model for its high capacity to non-specifically adsorb on hydrophobic surfaces. In order to characterize the anti-biofouling role of GO, contact angle hysteresis and contact angle under electrowetting measurements of a droplet containing GO/BSA are performed. Electrowetting has been selected because it is the most sensitive technique to non-specific adsorption: surface pollution is directly linked to the CA modification reversibility. The latter will be the major indication of surface biopollution. The results presented here could be applied to other microfluidic systems, either continuous, droplet-based or digital ones.

Materials and methods

Graphene oxide (GO) nanosheets were obtained using the modified Hummers' method.[23,24] The GO nanosheets were characterized in our previous work[25,26] by X-ray photoelectron spectroscopy (XPS) and atomic force microscopy (AFM). XPS analysis indicates that the GO nanosheets comprise oxygen containing groups such as hydroxyl (C–OH), epoxide (C–O–C), carbonyl (C=O) and carboxyl (COOH). The presence of these groups on the GO surface confers an amphiphilic character to GO. GO nanosheets are easily dispersible in polar solvents like water or alcohols.[27] AFM characterization is made on a mica substrate where droplets containing GO were evaporated. These measurements show that the characteristic length of the nanosheets is about 300 nm and their thickness is 0.4–0.5 nm.[25,26] The GO nanosheets are suspended in deionized water (DI water, $\rho = 18.2$ MΩ cm^{-1}) and mixed with rhodamine-labeled BSA (Interchim, France) through a vortex mixer in order to obtain a homogeneous solution.

Contact angle hysteresis measurements were performed on a silicon wafer (⟨100⟩, n-doped, resistivity: 5–10 Ω cm^{-1}, Siltronix, France) recovered by a spin-coated hydrophobic 30 nm thick Cytop® layer (AGC Chemicals, Asahi Glass Co., Ltd, Japan).

Electrowetting experiments were performed on a SU-8 spin-coated silicon wafer (⟨100⟩, n-doped, resistivity: 0.009–0.01 Ω cm^{-1}, Siltronix, France) recovered by a spin-coated hydrophobic Cytop® layer.

Contact angles of a 6 μL droplet were measured using a goniometer (DSA 100, Krüss GmbH, Germany) with its tilting table and its droplet analysis software. Contact angle hysteresis is calculated as the difference, at the triple contact line (TCL), between the advancing and the receding contact angles just before the contact line depinning during tilting (0.5° per second). In some cases when the TCL is stuck on the surface and the tilting table is set to 90° (vertical position), no droplet sliding is observed. The CAH is then estimated by the difference between the advancing and receding angles knowing that this estimation lowers the real value. This situation is indicated by the term 'no droplet sliding' at a tilting angle of 90°.

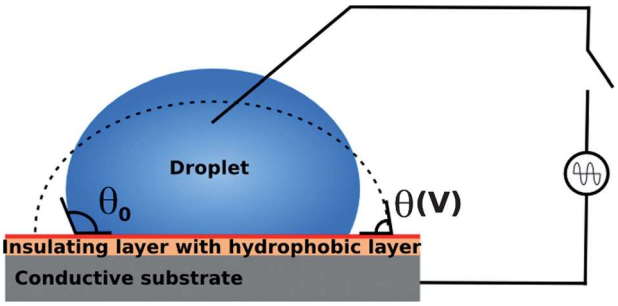

Fig. 1 Static electrowetting on the dielectric (EWOD) setup.

EWOD experiments were realized using a classical static setup with a hydrophobic conductive needle (Fig. 1). The voltage is generated by a signal generator (AFG320, Tektronix Inc., United States) coupled to a 50 dBm high-voltage amplifier (Model 2340, Tegam Inc., United States) and applied between the conductive droplet through the metallic, hydrophobic needle, and the conductive substrate. The voltage is a 1 kHz-squared signal with V_{eff} ranging from 25 to 212 V at the amplifier output.

The CA reversibility under EWOD is studied for BSA aqueous solutions (195 and 260 ng μL^{-1}), GO aqueous solutions (100 and 500 ng μL^{-1}) and BSA + GO aqueous solutions, using the following protocol:

(1) A droplet (6 ± 0.1 μL) is placed on the surface using a micropipette, then the needle is placed at the center of the droplet in order to penetrate sufficiently into the liquid to keep the contact with the droplet during its spreading;

(2) A voltage ($V_{eff} = 200$ V) is applied for 0.5 s to the droplet;

(3) The voltage is released after 0.5 s;

(4) Steps 2 and 3 are repeated ten times at the same voltage;

(5) The droplet is then released;

(6) DI water droplet (6 ± 0.1 μL) is placed at the same place to measure the contact angle modification due to BSA or GO adsorption.

In this experiment, the contact angle is measured every 0.1 s.

The evolution of the contact angle as a function of the applied voltage (voltage hysteresis) is also investigated using the following protocol:

(1) A droplet (6 ± 0.1 μL) is placed on the surface using a micropipette, then the needle is placed at the center of the droplet in order to penetrate sufficiently in the liquid to keep the contact with the droplet during its spreading;

(2) The contact angle is measured;

(3) The applied voltage is increased by steps of approximately 22 V;

(4) Steps 2 and 3 are repeated until the applied voltage reaches $V_{eff} = 212$ V;

(5) The applied voltage is decreased;
(6) The contact angle is measured;
(7) Steps 5 and 6 are repeated until $V_{eff} = 0$ V.

The EWOD hysteresis (H_{EW}) is then determined by calculating the maximum difference between the contact angle when the applied voltage is increased and the contact angle when the applied voltage is decreased. All the experiments are realized in triplicate and the mean values and standard deviations are calculated.

Results and discussion

Wetting properties: contact angle hysteresis

To study the influence of GO on BSA adsorption on the EWOD electrode surface, we have characterized the contact angle hysteresis of droplets of deionized water and droplets containing either GO, BSA or a mixture of GO–BSA at different ratios. We measured the CAH for two BSA concentrations (195, 260 ng μL^{-1}) supplemented with either 0, 100 or 500 ng μL^{-1} of GO.

Two behaviors can be distinguished from the CAH measurements (Fig. 2a). For both BSA solutions without GO or with a low concentration of GO (100 ng μL^{-1}), CAH measurements are estimated to be higher than 25°: CAH cannot be precisely determined because no sliding droplet can be observed even with a tilting angle of 90°. The indicated values are calculated from the difference between the advancing and receding angles at the maximum tilting angle. In these cases, there is a strong pinning of the TCL due to the surface modification by protein adsorption. A different behavior was observed for both BSA concentrations with 500 ng μL^{-1} of GO. The CAH decreased by a factor 4–5, down to 5–7° with standard deviations of about 2° and 4° for BSA concentrations of 195 ng μL^{-1} and 260 ng μL^{-1} and the tilting angles are equal to 15 ± 1° and 18 ± 1°, respectively. These values are lower than the CAH (10 ± 3°) and the tilting angle (25 ± 3°) of a deionized water droplet. This behavior is most likely due to the strong BSA adsorption on GO. BSA molecules are thus maintained in suspension inside the liquid droplet and are not transferred onto the hydrophobic surface.

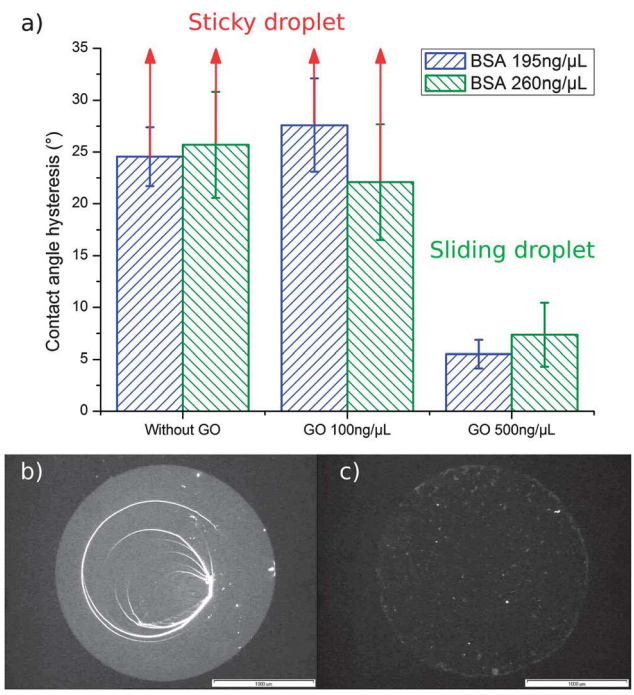

Fig. 2 (a) Contact angle hysteresis as a function of GO and BSA concentrations, 195 ng μL^{-1} in blue and 260 ng μL^{-1} in green. For GO concentrations of 0 and 100 ng μL^{-1}, no droplet sliding occurs at a tilting angle of 90°, (b) fluorescence images after CAH measurements for 195 ng μL^{-1} of BSA and (c) 195 ng μL^{-1} of BSA and 100 ng μL^{-1} of GO (length scale: 1000 µm). No fluorescence has been observed for 195 ng μL^{-1} of BSA and 500 ng μL^{-1} of GO.

To confirm the adsorption of BSA at the TCL for both GO concentrations, we used fluorescence to visualize the adsorbed BSA on the hydrophobic surface once the CAH has been measured and the droplet released.

Fig. 2b and c illustrate this adsorption for a 195 ng μL^{-1} BSA concentration. Fluorescence images are obtained only for droplets containing BSA with and without 100 ng μL^{-1} of GO. As expected, the fluorescence intensity is uniform and intense for a pure BSA droplet (Fig. 2b), and strongly decreases once 100 ng μL^{-1} of GO (Fig. 2c) is added with a more heterogeneous intensity. In that case, the fluorescence intensity is linked to the BSA adsorption level on the surface. For a higher GO concentration (500 ng μL^{-1}), no fluorescence intensity can be detected. From these observations, we can conclude that fluorescence is just related to the BSA adsorption. The addition of a low concentration of GO reduces BSA adsorption, but there is not enough free BSA to induce triple contact line pinning. For high GO concentrations, all BSA is adsorbed on GO and thus no pinning due to BSA accumulation was observed.

A similar behavior was observed in our previous publication:[17] for a [BSA]/[GO] lower than 0.5, the GO concentration is sufficient to adsorb BSA and to reduce the interaction between the liquid and the surface.

Electrowetting properties: reversibility

In order to characterize the influence of GO concentration on BSA biofouling, we investigated the reversible behavior of the liquid droplets of BSA/GO after 10 EWOD cycles. We define:

– θ_0 as the Young angle, contact angle before the application of a voltage;

– θ_1 as the contact angle when the voltage is applied for the first EWOD cycle;

– θ_2 as the contact angle when the voltage is released.

In the case of DI water (Fig. 3a), the EWOD effect is, as expected, reversible maintaining a CA θ_2, once the applied voltage is released, equal to θ_0 (110–112°). A 200 V applied voltage led to a decrease of the contact angle θ_1 quasi stable around 75–80° whatever the number of EWOD cycles.

For a droplet containing 100 ng μL^{-1} of GO (Fig. 3a), an overall reversible EWOD effect is observed. Starting with a Young angle θ_0 (115°), 5° higher than that for DI water, during the first 6 EWOD cycles, the θ_1 angle is maintained at 105–107° with a θ_2 angle between 75° and 80°. During the seventh EWOD cycle, a stall curve of about 7° (decreasing down to 70°) is observed compared to θ_0. As θ_2 can be seen as the receding angle

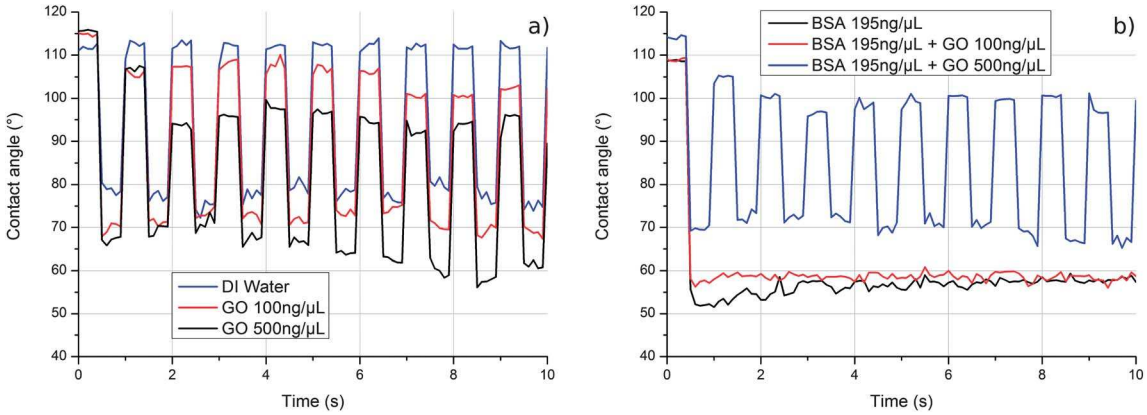

Fig. 3 10 EWOD cycles @ 200 V_{eff} for a 6 μL droplet containing (a) DI water (blue), 100 ng μL^{-1} (red), and 500 ng μL^{-1} (black) of GO; (b) BSA at 195 ng μL^{-1} without GO (black), with 100 ng μL^{-1} (red) and 500 ng μL^{-1} (blue) of GO.

under EWOD, its modification is assuredly due to the defects present on the surface. This minor defect may result from the accumulation of GO at the triple line (cumulative effect after 6 EWOD cycles on the same location). Nonetheless, it doesn't lead to a TCL pinning and thus allows a reversible EWOD effect.

For 500 ng μL^{-1} of GO (Fig. 3a), we observed during the first cycle a reversible EWOD effect, identical to the one observed for the 100 ng μL^{-1} GO concentration. Modification of θ_2, the receding angle under EWOD, appears earlier during the experiment, from the second cycle: the same stall curve of more than 10° with a decrease of θ_2, which remains between 90 and 95° and a progressive decrease of θ_1 from 70° to 58°. These first observations show that even the static EWOD cycle induces most likely GO accumulation at the triple line, and it does not lead to the pinning of the TCL during EWOD, thus allowing a reversible EWOD effect.

The next step consists of the addition of BSA to the droplet. For a BSA concentration of 195 ng μL^{-1} (Fig. 3b) without GO, the Young contact angle θ_0 is equal to 109°. Once the voltage is applied, the contact angle decreases sharply to θ_1 equal to 52–57°, and even if the voltage is released, the contact angle remains constant. In that case $\theta_1 = \theta_2$, meaning that the TCL is pinned due to proteins' adsorption on the surface.

Adding a small amount of GO (100 ng μL^{-1}) for a BSA concentration of 195 ng μL^{-1} (Fig. 3b) provokes the same irreversible EWOD effect *i.e.* $\theta_1 = \theta_2$ and is equal to θ_2 (57–60°). In such cases, the GO concentration is not sufficient to maintain all the BSA in suspension. BSA molecules that are not adsorbed on GO stick onto the hydrophobic surface, leading to a strong TLC pinning.

Increasing the GO concentration up to 500 ng μL^{-1} changes the droplet response. For a BSA concentration of 195 ng μL^{-1}, starting from a Young angle of $\theta_0 = 114°$, during the 10 EWOD cycles, θ_1 remains constant at 70°, while θ_2 is about 100°. The contact angle variation, due to the applied voltage, is 30°. In that case, BSA is adsorbed preferentially on GO sheets and not on the surface. The EWOD effect is reversible and the TCL is not pinned. At a higher BSA concentration (260 ng μL^{-1}, Fig. S1†) with the GO of 500 ng μL^{-1}, the EWOD becomes reversible. Nonetheless, while θ_1 remains relatively stable at 75°, θ_2 varies strongly with a mean value of 95 ± 7°. This behavior can be explained by the fact that the droplet contains a high concentration of BSA compared to the results in Fig. 3a, for the same GO concentration. Saturation of the adsorption of BSA on GO is observed in that case, leading to a partial retractation of the TCL once the voltage is released.

In order to assess the biofouling of the surface, once the 10 EWOD cycles are performed, the droplet is released and a fresh DI water droplet is deposited on the same place. Then, the contact angle is measured to detect any surface modification induced by BSA adsorption during EWOD cycles. The results are presented in Fig. 4. As expected for a water droplet deposited on the hydrophobic surface containing BSA and GO (concentration of 0 or 100 ng μL^{-1}), the measured contact angles are between 60° and 70° for 195 and 260 ng μL^{-1} of BSA, far lower than the initial value of the Cytop® surface (Young angle = 112°). As observed in Fig. 4, for both BSA concentrations (195 and 260 ng μL^{-1}) without and with 100 ng μL^{-1} of GO, there is a surface property modification due to protein adsorption,

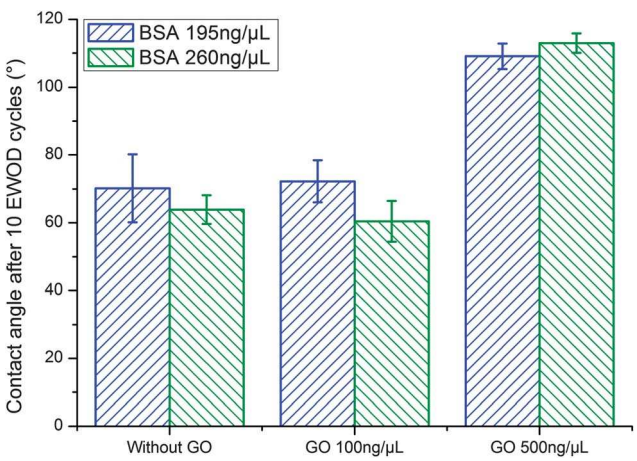

Fig. 4 Contact angle of a DI water droplet after 10 EWOD cycles *vs.* GO concentration, 195 (blue) and 260 ng μL^{-1} (green) of BSA.

leading to an irreversible EWOD behavior and to a modification of the surface wettability. However, when the GO concentration is significantly increased to 500 ng μL^{-1}, the contact angle of a DI droplet, after 10 EWOD cycles, is equal to 110°, similar to the initial Young angle of the Cytop® surface. It confirms that no surface wettability change occurred and that reversible EWOD behavior can be achieved at this BSA concentration. BSA adsorption on GO nanosheets prevents BSA adsorption on the surface and avoids protein biofouling.

It should be noted that beyond the characterization of the wetting properties under static electrowetting, the overall objective is to displace biomolecules thanks to a monophasic droplet based system. As far as EWOD is concerned, the droplet displacement requires just one EWOD cycle on one electrode for its motion to the next electrode. Thus, even if the accumulation of GO nanosheets at the TCL (Fig. 4) led to a diminution of the CA reversible modification after the second EW cycle, it can be considered as negligible within EWOD based droplet motion.

Electrowetting properties: voltage hysteresis

We have examined the evolution of the contact angle during EWOD with respect to the applied voltage (V_{eff}). We first investigated pure DI water and droplets of water containing 100 and 500 ng μL^{-1} of GO (Fig. 5a). For DI water, the contact angle decreases continuously from 113° to 76° when the applied voltage is increased. Then, when the applied voltage is decreased, the contact angle increases continuously from 76° to 109°. We define electrowetting hysteresis (H_{EW}) as the difference between the contact angles upon increasing and decreasing the applied voltage for the same value. H_{EW} is between 0° and 6°. With 100 ng μL^{-1} of GO, the contact angle also decreases continuously with an increasing voltage, from 113° to 70°. The contact angle increases continuously from 66° to 103° upon decreasing the voltage. In this case, H_{EW} is between 0° and 13°. With a higher GO concentration (500 ng μL^{-1}), the contact angle varies from 114° to 64° when the applied voltage is increased. When the applied voltage is decreased, the contact angle increases from 59° to 96°, corresponding to H_{EW} between 0° and 18°.

We clearly observe an effect due to the presence of GO nanosheets like the one already reported in Fig. 3a (electrowetting cycles). The threshold voltage required to decrease significantly the contact angle is lower with GO solutions than DI water and decreases when the GO concentration increases (22 V for 100 ng μL^{-1} and 500 ng μL^{-1} of GO and 72 V for DI water). Furthermore, GO allows a larger contact angle variation at a high applied voltage. However, when the applied voltage is decreased, a non-monotonous behavior is observed. As mentioned before, this might be due to the interactions between GO nanosheets and the surface, inducing a TLC slight pinning: the receding angle under EWOD is largely modified in that case.

Concerning the tests with pure BSA liquids, with a 195 ng μL^{-1} concentration (Fig. 5b), the contact angle decreases continuously from about 105° to 55°, when the applied voltage is increased. However, during the decrease of the applied voltage, the contact angle remains constant around 57–58°. This leads to a high H_{EW} (50°) and TLC pinning. With the same BSA concentration (195 ng μL^{-1}) mixed with 100 ng μL^{-1} of GO, the droplet response under EWOD is quite similar to BSA solutions, except that the resulting hysteresis is a few degrees lower.

Upon increasing the GO concentration, a huge diminution of the voltage hysteresis is observed. For 500 ng μL^{-1} of GO and 195 ng μL^{-1} of BSA, while the contact angle decreases from 116° to 70° during the applied voltage increase, the contact angle increases from 70° to 99° when the applied voltage is decreased. In this case, H_{EW} is between 0° and 17°.

Similar observations have been made for a higher concentration of BSA (260 ng μL^{-1}, Fig. S2 in ESI†). These experiments confirm the previous results obtained with EWOD cycles. Without or with a small amount of GO, BSA adsorbs on the surface than on the GO nanosheets leading to an irreversible TCL pinning. Nonetheless, with a higher amount of GO, BSA is preferentially adsorbed on the GO nanosheets; the TCL can be depinned.

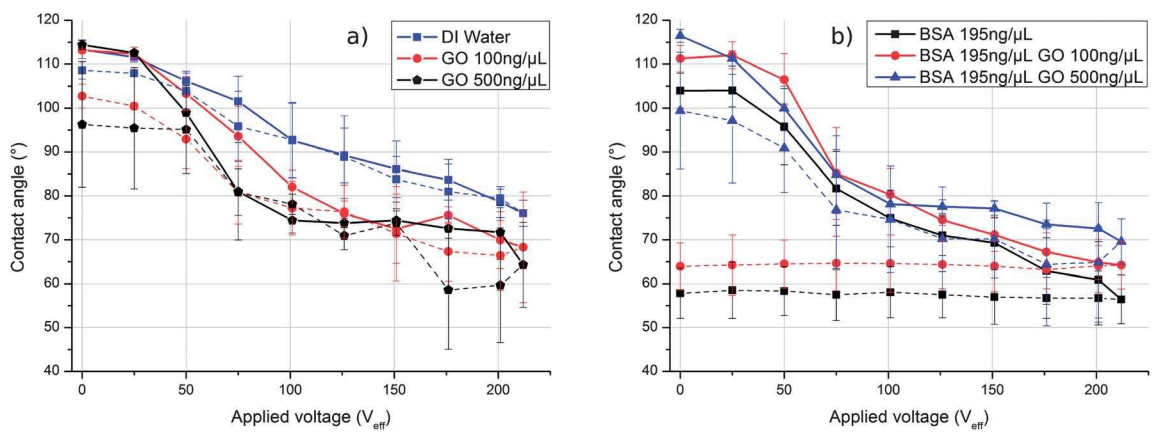

Fig. 5 Contact angle *vs.* applied voltage for (a) DI water (blue), with 100 ng μL^{-1} (red) and 500 ng μL^{-1} (black) of GO; (b) BSA at 195 ng μL^{-1} without GO (black), with 100 ng μL^{-1} (red) and 500 ng μL^{-1} (blue) of GO, solid line for increasing voltage and dashed line for decreasing voltage.

Conclusion

We have characterized the influence of graphene oxide aqueous solution on the surface biofouling by a hydrophobic protein BSA. In order to qualitatively determine the pollution level, wetting and electrowetting properties were investigated. Indeed, these properties are largely dependent on the quality of the surface because a low level of non-specific adsorption usually leads to a TCL strong pinning inducing a high CAH and a non-reversible EWOD effect under the applied voltage. Firstly, the CAH measurements show that the presence of GO sheets with BSA decreases the CAH to a value inferior to the hysteresis developed by a water droplet. This suggests the non-adsorption of GO sheets loaded or unloaded with BSA on the surface. The wetting properties are clearly enhanced by GO nanosheets. Then, in order to investigate the electrowetting properties, two tests have been performed, either by switching the voltage or by the hysteresis voltage cycle. As expected, aqueous droplets containing BSA (195 and 260 ng μL^{-1}) exhibit a non-reversible behavior, synonymous of protein biofouling and triple contact line irreversible pinning. Once GO nanosheets are added, an influence of its concentration level is observed: above a ratio of [BSA]/[GO] equal to 0.5, proteins adsorb on the surface and strongly modify the electrowetting behavior (irreversible TCL pinning), while for a lower ratio, electrowetting properties are maintained non or weak biofouling. These characterizations confirm the results presented in our previous work and prove that GO is an interesting alternative to prevent biofouling, avoiding surface engineering,[28,16] not only for EWOD, but for microfluidics in general. In the future work, we will focus on coupling EWOD displacement with biodetection or analysis. Two solutions can be investigated, either the direct analysis of proteins on the GO by mass spectrometry, after an evaporation step, as already demonstrated by Tang *et al.*[19] or to develop strategies to locally release proteins from GO in order to operate in line analysis/detection. For the latter solution, we can mention a specific interaction of the BSA, in our case, with a high affinity molecule immobilized on the surface or to modify pH and/or the ionic strength solution of the droplet in order to enhance the electrostatic repulsion between BSA and GO. The effect of the pH and ionic strength as well as the chemical composition of GO (degree of oxidation/reduction) on the surface biofouling is currently under investigation in our laboratory.

Acknowledgements

We acknowledge gratefully the European Regional Development Fund (INTERREG IVa FW1.1.9 "Plasmobio" project), the Centre National de la Recherche (CNRS), the Université Lille 1 and the Nord Pas de Calais region for financial support.

References

1 M. J. Jebrail, M. S. Bartsch and K. D. Patel, *Lab Chip*, 2012, **12**, 2452–2463.
2 K. Choi, A. H. C. Ng, R. Fobel and A. R. Wheeler, *Annu. Rev. Anal. Chem.*, 2012, **5**, 413–440.
3 C. Delattre, P. Allier, Y. Fouillet, D. Jary, F. Bottausci, D. Bouvier, G. Delapierre, M. Quinaud, A. Rival, L. Davoust and C. Peponnet, *Biosens. Bioelectron.*, 2012, **36**, 230–235.
4 R. Mukhopadhyay, *Anal. Chem.*, 2005, **77**, 429A–432A.
5 J. Atencia and D. J. Beebe, *Nature*, 2005, **437**, 648–655.
6 M. W. Toepke and D. J. Beebe, *Lab Chip*, 2006, **6**, 1484–1486.
7 F. Mugele and J.-C. Baret, *J. Phys.: Condens. Matter*, 2005, **17**, R705–R774.
8 F. Li and F. Mugele, *Appl. Phys. Lett.*, 2008, **92**, 4108.
9 A. P. Aijian, D. Chatterjee and R. L. Garrell, *Lab Chip*, 2012, **12**, 2552–2559.
10 V. N. Luk, G. C. Mo and A. R. Wheeler, *Langmuir*, 2008, **24**, 6382–6389.
11 S. H. Au, P. Kumar and A. R. Wheeler, *Langmuir*, 2011, **27**, 8586–8594.
12 R. B. Fair, *Microfluid. Nanofluid.*, 2007, **3**, 245–281.
13 D. Brassard, L. Malic, F. Normandin, M. Tabrizian and T. Veres, *Lab Chip*, 2008, **8**, 1342–1349.
14 S.-K. Fan, Y.-W. Hsu and C.-H. Chen, *Lab Chip*, 2011, **11**, 2500–2508.
15 F. Lapierre, G. Piret, H. Drobecq, O. Melnyk, Y. Coffinier, V. Thomy and R. Boukherroub, *Lab Chip*, 2011, **11**, 1620–1628.
16 M. Jönsson-Niedziółka, F. Lapierre, Y. Coffinier, S. J. Parry, F. Zoueshtiagh, T. Foat, V. Thomy and R. Boukherroub, *Lab Chip*, 2011, **11**, 490–496.
17 G. Perry, V. Thomy, M. R. Das, Y. Coffinier and R. Boukherroub, *Lab Chip*, 2012, **12**, 1601–1604.
18 M. Zhang, B. Yin, X. Wang and B. Ye, *Chem. Commun.*, 2011, **47**, 2399–2401.
19 L. A. L. Tang, J. Z. Wang and K. P. Loh, *J. Am. Chem. Soc.*, 2010, **132**, 10976–10977.
20 Y. Lu, H. Kong, F. Wen, S. Zhang and X. Zhang, *Chem. Commun.*, 2013, **49**, 81–83.
21 S. S. Chou, M. De, J. Y. Luo, V. M. Rotello, J. X. Huang and V. P. Dravid, *J. Am. Chem. Soc.*, 2012, **134**, 16725–16733.
22 K. P. Loh, Q. L. Bao, G. Eda and M. Chhowalla, *Nat. Chem.*, 2010, **2**, 1015–1024.
23 W. S. Hummers and R. E. Offeman, *J. Am. Chem. Soc.*, 1957, **80**, 1339.
24 M. R. Das, R. K. Sarma, R. Saikia, V. S. Kale, M. V. Shelke and P. Sengupta, *Colloids Surf., B*, 2011, **83**, 16–22.
25 I. Kaminska, M. R. Das, Y. Coffinier, J. Niedziolka-jonsson, P. Woisel, M. Opallo, S. Szunerits and R. Boukherroub, *Chem. Commun.*, 2012, **48**, 1221–1223.
26 O. Fellahi, M. R. Das, Y. Coffinier, S. Szunerits, T. Hadjersi, M. Maamache and R. Boukherroub, *Nanoscale*, 2011, **3**, 4662–4669.
27 L. J. Cote, J. Kim, V. C. Tung, J. Y. Luo, F. Kim and J. X. Huang, *Pure Appl. Chem.*, 2011, **83**, 95–110.
28 P. Y. Yeh, Z. Zhang, M. Lin and X. Cao, *Langmuir*, 2012, **28**, 16227–16236.

